Naval Research Laboratory
Washington, DC 20375-5320

U.S. NAVAL RESEARCH LABORATORY

NRL/6850/MR—2024/1

Lattice-Matched Epitaxial III-N / M_2AN Alloy Heterostructures

Douglas S. Katzer

Neeraj Nepal

Matthew T. Hardy

Electromagnetic Technology Branch
Electronics Science and Technology Division

January 12, 2024

DISTRIBUTION STATEMENT A: Approved for public release; distribution is unlimited.

REPORT DOCUMENTATION PAGE

PLEASE DO NOT RETURN YOUR FORM TO THE ABOVE ORGANIZATION

1. REPORT DATE	**2. REPORT TYPE**	**3. DATES COVERED**	
12-01-2024	NRL Memorandum Report	**START DATE** 10/01/2019	**END DATE** 09/30/2023

4. TITLE AND SUBTITLE
Lattice-Matched Epitaxial III-N / M2AN Alloy Heterostructures

5a. CONTRACT NUMBER	**5b. GRANT NUMBER**	**5c. PROGRAM ELEMENT NUMBER**
5d. PROJECT NUMBER	**5e. TASK NUMBER**	**5f. WORK UNIT NUMBER**
		1L59

6. AUTHOR(S)
Douglas Scott Katzer, Neeraj Nepal, and Matthew T. Hardy

7. PERFORMING ORGANIZATION / AFFILIATION NAME(S) AND ADDRESS(ES)	**8. PERFORMING ORGANIZATION REPORT NUMBER**
Naval Research Laboratory 4555 Overlook Ave SW Washington, DC 20375-5320	NRL/6850/MR—2024/1

9. SPONSORING / MONITORING AGENCY NAME(S) AND ADDRESS(ES)	**10. SPONSOR / MONITOR'S ACRONYM(S) NUMBER**	**11. SPONSOR / MONITOR'S REPORT NUMBER(S)**
Office of Naval Research 875 N. Randolph Street Arlington, VA 22203-1995	ONR	

12. DISTRIBUTION / AVAILABILITY STATEMENT
DISTRIBUTION STATEMENT A: Approved for public release; distribution is unlimited.

13. SUPPLEMENTAL NOTES

14. ABSTRACT

15. SUBJECT TERMS

16. SECURITY CLASSIFICATION OF:			**17. LIMITATION OF ABSTRACT**	**18. NUMBER OF PAGES**
a. REPORT	**b. ABSTRACT**	**c. THIS PAGE**	SAR	14
U	U	U		

19a. NAME OF RESPONSIBLE PERSON	**19b. PHONE NUMBER** *(Include area code)*
Douglas Katzer	(202) 767-2523

This page intentionally left blank.

CONTENTS

1. INTRODUCTION 3
   1.1 Objective and Motivation 3
   1.2 Background 3
2. APPROACH 5
3. RESULTS AND DISCUSSION 5
   3.1 TiN and TiAlN alloys 5
   3.2 TaN_x and TaAlN alloys 6
   3.3 Substrate temperature rise and mitigation 7
   3.4 III-N polarity control on TMNs 9
4. CONCLUSIONS 10
5. REFERENCES 11

This page intentionally left blank.

EXECUTIVE SUMMARY

This report presents a summary of the findings for the U. S. Naval Research Laboratory 6.1 basic research program Work Unit 1L59/991L59 on "Lattice-Matched Epitaxial III-N / M_2AN Alloy Heterostructures." Substantial progress was made in the molecular-beam epitaxial (MBE) growth of transition metal nitride (TMN) thin films of TiN, NbN, and TaN, as well as growth of Ti_2AlN and Ta_2AlN M_2AN alloy materials. Greater understanding of the substrate temperature rise induced during growth of low emissivity metals on high emissivity substrates like sapphire and SiC was developed, along with new engineered absorbing layers to increase the radiative thermal coupling between the substrate heater and the substrate. New reproducible techniques were created to grow metal-polar III-N films on top of TMN films – overcoming the natural tendency for III-N films to be N-polar on TMNs. The results in this program contributed several presentations at scientific meetings, publications in scientific journals, and to follow-on 6.1 and 6.2 research programs inside of NRL as well as ongoing and new externally funded research efforts.

This page intentionally left blank.

LATTICE-MATCHED EPITAXIAL III-N / M_2AN ALLOY HETEROSTRUCTURES

1. INTRODUCTION

1.1 Objective and Motivation

The scientific objective of this basic research project was to explore and create high-quality molecular-beam epitaxial (MBE) growth of new epitaxial M_2AN transition metal nitride (TMN) thin films and heterostructures that are nearly lattice-matched to group III-N materials, and to characterize their morphology, structure, and electronic properties. These new epitaxial metals will enable the creation of devices such as metal base transistors that were first described in the 1960s but could not be fabricated because of the difficulty in growing high-quality semiconductors on metals. Understanding and controlling III-N/TMN interface formation, the substrate heating effects induced by epitaxial metal growth changing the thermal emission characteristics, and controlling the overgrown III-N crystal polarity are essential for using these epitaxial materials in practical applications. These new epitaxial materials also will enable advances in wide bandgap GaN transistor technology through advanced processing capabilities, such as selective etching and lift-off of processed devices from their native growth substrate and transfer onto other materials for improved heat sinking or for integration with other electron device technologies. Success in this program will ultimately enable the development of advanced electronic devices with higher power output density, higher operating temperature capability, reduced size necessary to meet array packing requirements, superior RF and mm-wave performance (higher gain, lower loss, increased bandwidth) for future Navy radar, EW, communications systems and related areas.

1.2 Background

Epitaxy is the deposition of ordered crystalline material on a crystalline substrate. In general, successful epitaxy requires: 1) similar crystalline structures between the substrate and epitaxial layer (e.g. cubic on cubic; hexagonal on hexagonal); 2) similar crystalline orientations (a- and c-axes mutually parallel); and 3) small (< 1%) mismatch in the in-plane lattice parameters ($a_l \approx a_s$). Lattice-matching is required the highest quality epitaxial film quality, the sharpest interfaces between the layers, and the ultimate electron device performance.

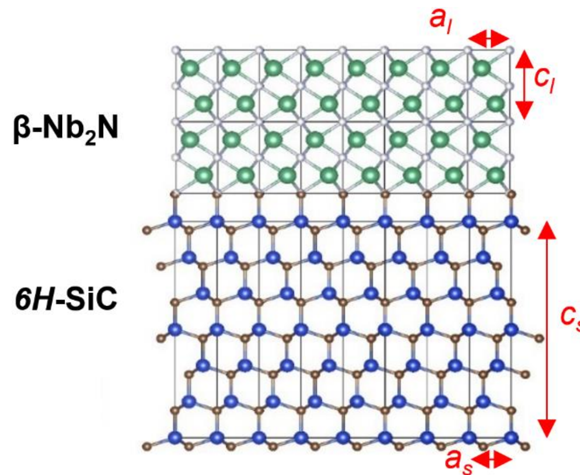

Fig. 1 — Model of an epitaxial hexagonal β-Nb_2N film on a hexagonal 6H-SiC substrate showing the respective *a*- and *c*-axis lattice parameters and unit cells.

Before this work was undertaken at NRL, there were few (if any) technologically useful metals which could lattice-match important group III-N semiconductors, and this limits high-performance electron device designs and system functionality. The lack of lattice-matching means that epitaxial layers would be highly strained resulting in generation of dislocations when the crystal relaxed. Dislocations are well

Manuscript approved January 11, 2024.

known causes of reduction of conduction electron velocity and mobility, reduction in thermal conductivity, increases in gate and p/n junction leakage, increases in impurity diffusion, and increases in electron trapping which reduces high-frequency device performance. In addition, the present lack of practical, robust metals in group III-N device technology leads to ohmic contact degradation at high temperatures. The most common gate metal in III-N HEMTs, nickel, is thermodynamically unstable in contact with III-N layers, leading to degraded device reliability and lifetime. Finally, these metal limitations means that one cannot fabricate novel devices that require epitaxial buried metal layers under semiconductor layers. All of these issues prompted this program to create high-quality epitaxial layers of M_2AN transition metal nitride alloys which are lattice-matched to III-N materials.

The M_2AN materials are part of the so-called MAX-Phase materials and are compelling for new epitaxial investigations because of their desirable structural and electronic properties. **M** represents a transition metal, **A** generally represents a group III element, and **X** is N or C.

H			M2AN Elements of Interest														He
Li	Be											B	C	N	O	F	Ne
Na	Mg											Al	Si	P	S	Cl	Ar
K	Ca	Sc	Ti	V	Cr	Mn	Fe	Co	Ni	Cu	Zn	Ga	Ge	As	Se	Br	Kr
Rb	Sr	Y	Zr	Nb	Mo	Tc	Ru	Rh	Pd	Ag	Cd	In	Sn	Sb	Te	I	Xe
Cs	Ba	Lu	Hf	Ta	W	Re	Os	Ir	Pt	Au	Hg	Tl	Pb	Bi	Po	At	Rn

Fig. 2 — Periodic table of the elements showing the M, A, and N elements of interest for M_2AN films in this program.

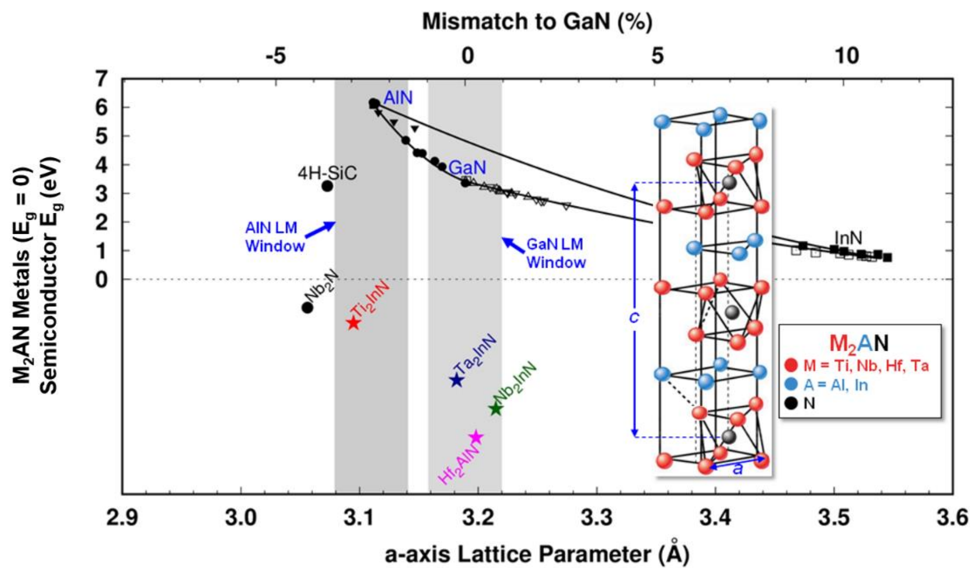

Fig. 3 — Semiconductor bandgap energy vs. in-plane lattice parameter for III-N semiconductor alloys and selected transition metal nitrides, SiC, and candidate M_2AN alloy materials. Inset shows M_2AN crystalline unit cell.

There are three **A** elements that were investigated for this program – Al, Ga, and In. Of these, In would be the most difficult to incorporate into the M_2AN film because of its high vapor pressure at the growth temperature needed for sufficient **M** atom surface mobility. In other words, extremely high In fluxes would need to be incident on the growing surface to have a fraction of the flux incorporate, and if it did

incorporate, the actual incorporation rate would be difficult to control. Of these three elements, we initially concentrated on Al as it has the lowest vapor pressure among them (10^{-5} mbar at 883 °C, vs 800 °C for Ga and 655 °C for In)[1].

2. APPROACH

Since the M_2AN materials are hexagonal (space group $P6_3/mmc$, #194), it makes sense to begin the growth studies by starting with similar hexagonal materials. Unfortunately, while a substantial body of literature exists on bulk M_2AC materials, M_2AN materials are less widely reported, and little has been reported to date on thin-films of M_2AN materials with the exception of sputtered Ti_2AlN[2,3]. For the binary constituents, TiN is cubic while AlN is usually hexagonal. While we have demonstrated hexagonal phase growth of binary NbN_x compounds, in particular hexagonal β-Nb_2N[4,5], to date it has been difficult to obtain uniform single-phase hexagonal Nb_2N – instead the cubic δ-NbN_x phase has usually been dominant for our growth conditions. Given these issues, it was decided to investigate Ti_2AlN for comparison to the literature, as well as to perform more detailed growth and characterization studies of hexagonal TaN_x– based alloys which we had previously found to be more reproducible and uniform than hexagonal Nb_2N, for M_2AN MBE materials growth and characterization.

TMN and M_2AN epitaxial films were grown by RF-plasma MBE using systems and processes described earlier[5]. Transition metal fluxes were generated by an in-situ multiple pocket electron beam evaporator (Nb, Ta) or a special high-temperature effusion cell with a liquid titanium compatible crucible (Ti). Films were characterized in-situ by reflection high-energy electron diffraction (RHEED), and ex-situ by a variety of techniques.

3. RESULTS AND DISCUSSION

3.1 TiN and TiAlN alloys

TiN and TiAlN alloys were grown by MBE on sapphire and SiC substrates by MBE. The TiN test films were grown using a growth rate of 0.1 Å/s and varying substrate temperatures. The TiN test film grown on sapphire was highly resistive, possibly indicating reaction between the Al_2O_3 substrate and the incident Ti flux, or that the growth temperature was lower than expected. The TiN films grown on SiC were reproducible and had similar characteristics to those reported by Richardson[6]. Of the Ti_2AlN films grown on SiC to date, these films have been mixtures of hexagonal AlN with cubic TiN grains with small fractions of the film being the desired Ti_2AlN phase.

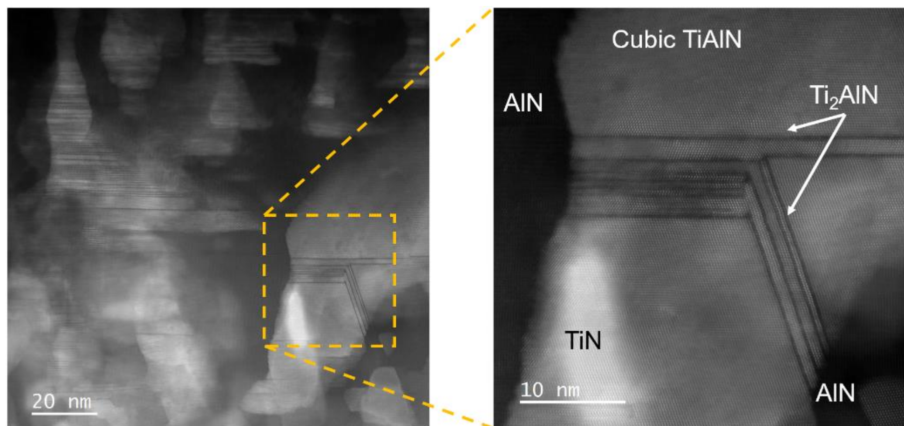

Fig. 4 — High resolution STEM imaging of MBE TiAlN film A255. Images indicate a grainy film composed of regions of cubic TiN, hexagonal AlN, cubic TiAlN, and small isolated black line segments of what appears to be hexagonal Ti_2AlN[7].

We hypothesize that there is a competition between sufficiently high temperatures for good Ti surface mobility and a low enough temperature for sufficient Al incorporation. Understanding and control of the substrate temperature of the substrate and growing film was a major challenge in this work and will be discussed in more detail below. TiAlN film A255 included a thin TiN buffer layer to enhance substrate heating and was mostly grown at a substrate thermocouple temperature of 900 °C. A later TiAlN film, A391, was grown without a TiN buffer layer at 1050 °C and shows a more a uniform grain structure, but no signs of the Ta_2AlN phase in STEM images – apparently as a result of reduced Al incorporation at the higher growth temperature. More work is needed to improve the film uniformity and increase the fraction of the Ta_2AlN phase, but there is a clear path forward for improving the MBE-grown Ti_2AlN films.

3.2 TaN_x and TaAlN alloys

We took advantage of our understanding of NbN_x MBE[4,5] to more rapidly climb the learning curve for TaN_x epitaxy[5,8]. The similarity of the equilibrium phase diagrams for Nb – N and Ta – N indicated that similar phases would be expected by simply shifting the TaN_x growth temperature to higher values – in particular, using ~ 100 °C higher growth temperature than NbN_x to compensate for the higher melting point of tantalum compared to niobium. Also, the greater separation – and lack of phase overlap – in nitrogen composition space between hexagonal Ta_2N and hexagonal TaN_x compared to hexagonal Nb_2N and cubic NbN_x seems to indicate that growing phase-pure hexagonal TaN_x is "easier" from a thermodynamics standpoint than growing phase pure Nb_2N. Single-phase epitaxial hexagonal TaN_x films were grown on 4H- and 6H-SiC substrates and characterized. Detailed STEM characterization and modeling indicates the TaN_x phase is the desired hexagonal γ-Ta_2N phase[5,9]. Interestingly, the Ta_2N films are nearly threading dislocation free when grown on SiC. Ordered planar defects caused by Ta vacancies were observed and characterized.

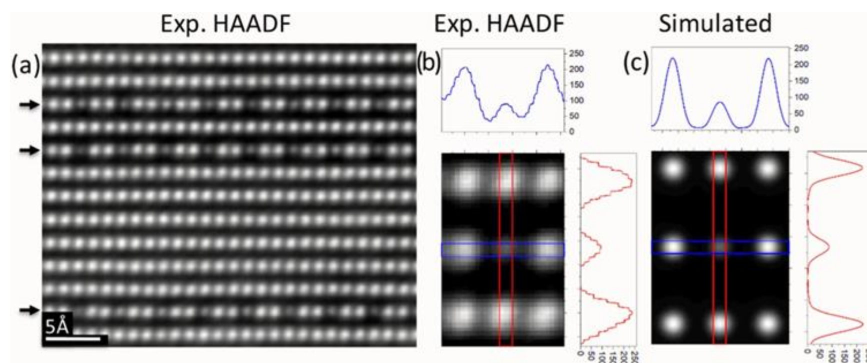

Fig. 5 — High resolution high-angle annular dark field (HAADF) imaging of MBE Ta_2N film P686. Images and modeling indicate the film is hexagonal γ-Ta_2N and ordered the planar defects related to Ta vacancies are observed[9].

Recently, A501, a TaAlN film on a Ta_2N buffer was grown on 4H-SiC. RHEED and XRD characterization indicate the films are of high quality, but seems to include an Al-rich phase. The film surface is smooth, having an rms roughness of 0.6 nm in AFM. TEM and atom-probe characterization of this sample are in progress.

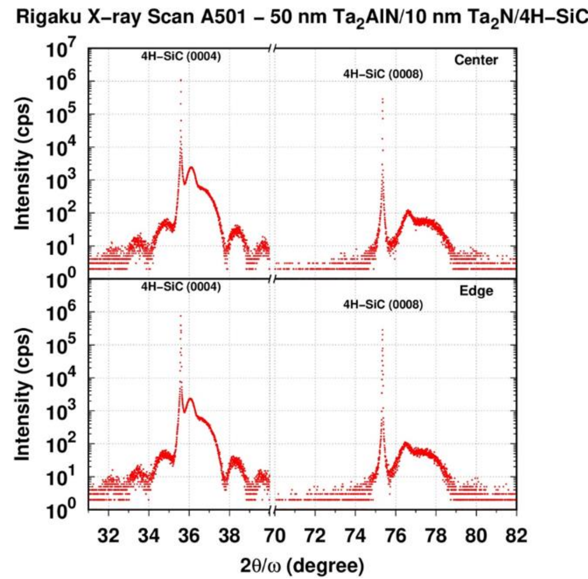

Fig. 6 — High resolution X-ray diffraction of sample A501 consisting of 50 nm TaAlN on 10 nm of Ta_2N on 4H-SiC.

Clear trends were observed in RHEED pattern smoothness and the presence or absence of surface reconstruction with increasing growth temperature. Sufficiently high substrate temperatures are required for streaky RHEED patterns, and the temperature required is higher for TaN_x than for NbN_x – apparently a consequence of the higher melting point for Ta compared to Nb. However, temperatures that are too high, at least for NbN_x with the active nitrogen fluxes used to date, cause rapid roughening of the center of the sample and rapid dimming of the RHEED pattern indicating damage to the film. This onset of damage has been consistently observed for NbN_x growth at substrate heater thermocouple temperatures above 1140 °C, while smooth TaN_x films are obtained at temperatures of 1140 °C and 1200 °C without any signs of damage in RHEED. Finally, **A** element incorporation is clearly limited at high growth temperatures, so the growth temperature of M_2AN films must be optimized and be low enough to obtain the desired alloy phase.

3.3 Substrate temperature rise and mitigation

As part of the growth studies of NbN_x and TaN_x, detailed temperature measurements were made to understand the evolution of the growth temperature during growth. This can be particularly important during the growth of metals (Eg = 0 eV) on wide bandgap semiconductors (SiC Eg ~ 3.26 eV) because the absorption of infrared (IR) energy from the substrate heater will dramatically increase for even very thin epitaxial metal films. In addition, the simple action of opening the main substrate shutter will lead to increased heat loss from the heater cavity and a drop in the substrate temperature even though the substrate heater thermocouple temperature is fixed. We were able to quantify these observations and found the substrate temperature increased ~ 240 °C after the growth of as little as 5 nm of NbN on 4H-SiC[10]. Since the M_2AN materials consist of refractory transition metal and group III metal alloys, it is critical to understand and control the temperature during growth as one must control potential reactions between the metals during the M_2AN epitaxial growth and be able to compensate for any excessive loss of the group III **A** flux during growth at high temperatures.

A common method to try to increase the IR coupling from the substrate heater into a transparent substrate is to use an opaque backside metal film (≈ 1 µm thick layer of Ti or TiW). This can enable the use of optical pyrometry to measure the backside metal temperature without it being overwhelmed by visible light from the heater. If a "two-color" (two wavelength) pyrometer is used, then the emissivity of the substrate can be compensated for *if* one can assume that the light that enters the pyrometer is only from

the substrate (and not from other hot sources like effusion cells[11]). However, opaque backside metal layers cannot be used with band-edge temperature measurements like diffuse reflectance spectroscopy which depend on observing non-specular reflection off the back surface[12]. In addition, Woltersdorff showed in 1934 that there is an optimum thickness of a metal layer to maximize IR absorption[13]. In particular, in the far IR where the optical parameters *n* and *k* are both large, the optimum metal thickness is such that the sheet resistance is half the characteristic impedance of free space (377/2 = 188.5 ohms/sq) which give a maximum absorbance of 0.5. So, thick metal layers should *not* be expected to be ideal to maximize substrate heating efficiency, and in general the optimum thickness will depend on temperature (via the dependence of IR emission on temperature).

MBE growth and temperature measurement experiments were undertaken using thin TiN absorber layers on 2" diameter SiC substrates in an attempt to optimize SiC substrate heating at high temperatures. Optical modeling using the "WPTherml" Python software package[14] was undertaken to examine the effect of the sheet resistance of the conducting TiN layer on the absorption of IR light from the substrate heater when operated at 1000°C (black body radiation peak ~ 2.5 µm).

Figure 7 shows the modeled reflectivity **R** (blue curves), transmittance **T** (yellow curves), emissivity / absorptivity **E, A** (green curves), and calculated thermal emission/absorption (red curves) for several modeled cases. Recall that **R** + **T** + **A** = **1**, and recall that in thermal equilibrium **A** = **E**. The left figure shows the calculations for a 1 µm thick layer of TiN on 4H-SiC at 1273K (1000 °C). Note that **T** is zero and the maximum **E** is only 18%. The center figure shows the calculated results for a 7 nm thick TiN layer on 4H-SiC. The peak **E** has increased to nearly 48%, illustrating the importance of optimizing the metal layer thickness for maximum **E**. Finally, the right figure shows the modeled results obtained for a thermal absorbing layer using 100 nm of Si on 10 nm of TiN on 4H-SiC. The peak **E** has increased to over 61%, giving a substantial increase over the bare TiN case.

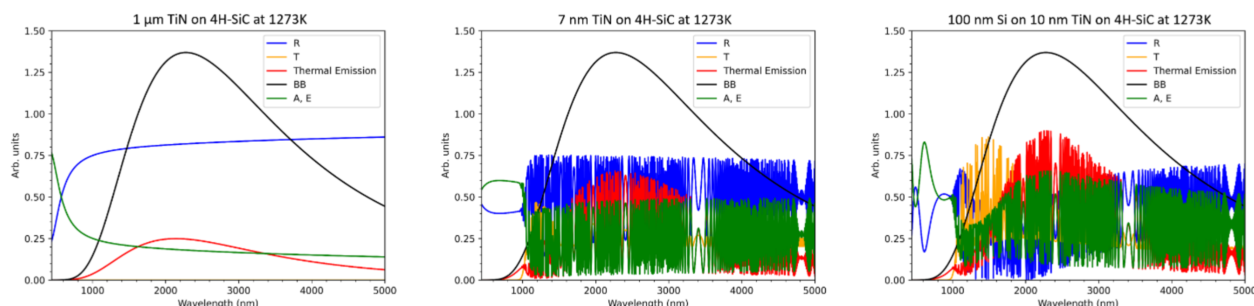

Fig. 7 — "WPTherml" models of (left) 1 µm TiN / 4H-SiC, (center) 7 nm TiN / 4H-SiC, (right) 100 nm Si / 10 nm TiN / 4H-SiC samples at 1273K. Thermal absorption/emission is maximized for thin single TiN layers (~ 7-10 nm thick), or for 100 nm Si / 10 nm TiN layers. Rapid Fabry–Pérot cavity oscillations can be seen in the thin TiN and Si/TiN cases.

Preliminary gallium desorption temperature measurement experiments indicated only a small temperature effect of the TiN metal thickness in the ≈ 1-100 nm thickness range on SiC, but extrinsic effects (differences in the Ga wettability of bare SiC between the samples) may be masking the temperature effects. However, an experiment adding ~ 100 nm of Si on top of the thin TiN layer led to a substantial increase in IR absorption with a clear temperature signature detected in RHEED. A true Si-face SiC surface temperature of ≈ 1000 °C (verified via a known RHEED transition from a 1x1 to an apparent (slightly C-rich surface) 1x3 at ≈ 1000 °C[15]) was obtained at a heater thermocouple temperature of only 1100°C for the TiN/Si absorber on SiC. (Note that the actual $(\sqrt{3}\times\sqrt{3})$-R30° reconstruction[16] appears to be a 1x3 reconstruction in the L_0 Laue zone visible in Figure 8 below.)

This work is continuing to verify the effect of the TiN/Si layers on 3" and 4" diameter substrates (which are even more difficult to heat to 1000 °C without an absorbing layer). These absorbing layers have wide

potential applicability including: 1) enabling higher-temperature growth of AlN with better control, 2) higher-temperature pre-epitaxial thermal cleaning of SiC, sapphire, AlN, and diamond substrates, 3) pre-hydrogenation surface preparation of diamond, 4) high-temperature SiC etching and flattening under a simultaneous Si flux. A publication discussing these findings is in preparation.

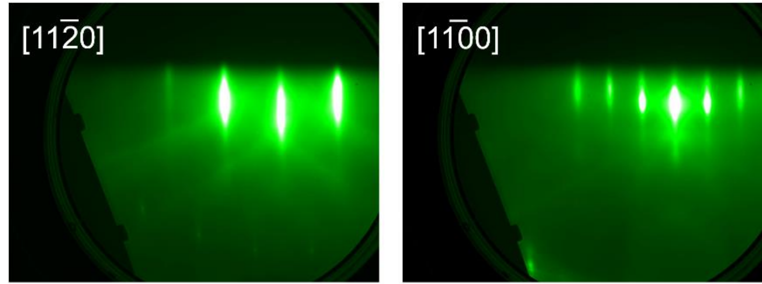

Fig. 8 — Apparent 1x3 surface reconstruction for SiC sample A497 with ~ 4 nm TiN and 100 nm Si absorber layer on backside, indicating real substrate temperature reached ≈ 1000 °C at 1100 °C thermocouple temperature. Actual surface reconstruction is (√3×√3)-R30° but the features are only visible in higher-order Laue zones[16].

3.4 III-N polarity control on TMNs

The hexagonal III-N semiconductors are polar materials which means that the top and bottom surfaces of a (0001)-oriented crystal are different. This crystal polarity affects the surface chemistry and electronic properties, and thus affects the properties of electron devices made on the two surfaces. To date, metal-polar III-N surfaces are preferred in most electron devices in the III-N semiconductors. However, with isolated exceptions, most III-N materials grown to date by MBE have been N-polar surfaces. Recent work has shown that as little as 1 nm of NbN can invert the polarity of Al-polar AlN to N-polar[17]. Careful growth experiments demonstrated that the polarity of III-N materials grown on AlN/TMN are not a function of the Al/N surface ratio in the AlN. That is – excess Al coverage on AlN will ***not*** convert the AlN polarity. While earlier results for AlN growth on Si indicates polarity inversion is determined by high levels of dopant impurities (e.g. Si) and the formation of an Al-Si-N eutectic [18,19], and demonstrates one method of intentional polarity inversion, this is not a well-controlled method and introduces potential adverse doping effects in overgrown transistors.

We have recently shown that high-quality metal-polar III-N heterostructures can be grown by MOCVD on MBE-grown TMN layers[20]. Close examination of the TEM data in that publication shows that the AlN nucleation layer is immediately Al-polar from the start of the growth on the NbN layer. Figure 9 shows a comparison of the measured cross-sectional image with a simple ball-and-stick crystal model. It is clear that the registry at the interface is via Al atoms sitting on the Nb site at the interface. Based on this evidence, we modified the growth conditions at the start of the AlN layer to include saturating the NbN surface with Al at high enough a substrate temperature to induce an exchange reaction to encourage Al to sit on Nb-sites. After the saturation was complete, the N-shutter was opened to continue the AlN growth.

It is often difficult to see a reconstruction on AlN surfaces in RHEED, so a thin GaN layer was grown on top of the AlN layer. As shown in Figure 9, a clear 2x2 reconstruction was obtained on the N-rich GaN surface, proving the GaN (and thus the underlying AlN) is metal polar.

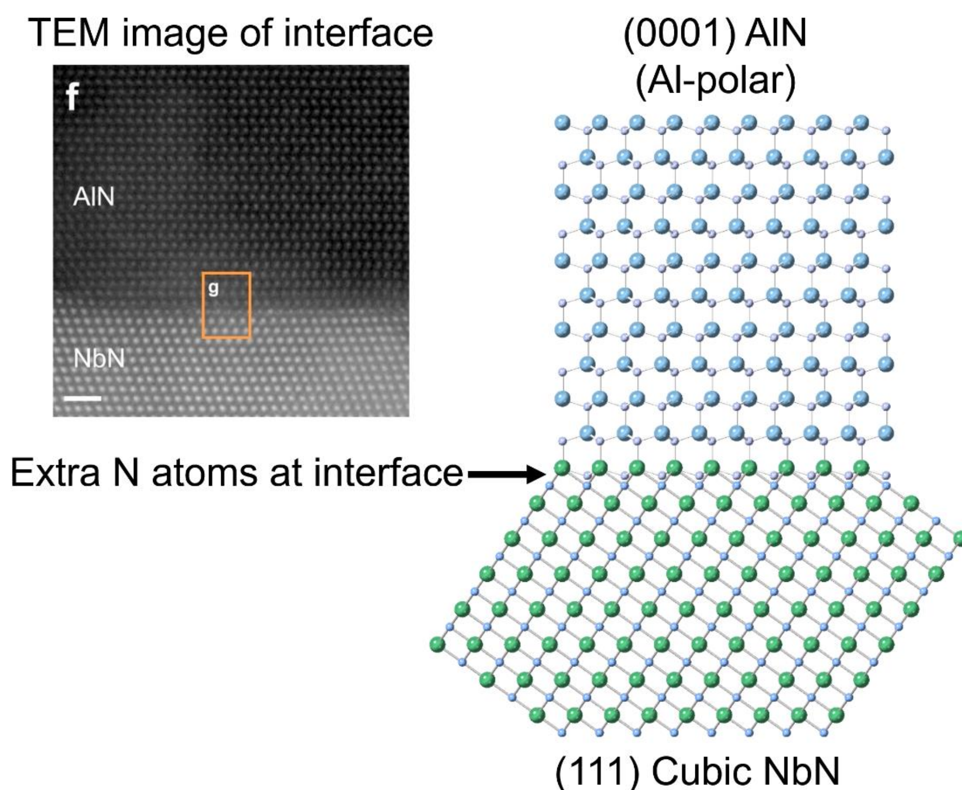

Fig. 9 — (Left) TEM image of MOCVD-grown AlN on NRL MBE NbN film[20]. TEM and electrical characteristics prove the film is Al-polar AlN. The image agrees with a ball-and-stick crystal model (right) if there is registry such that Al atoms sit on Nb-sites at the NbN surface.

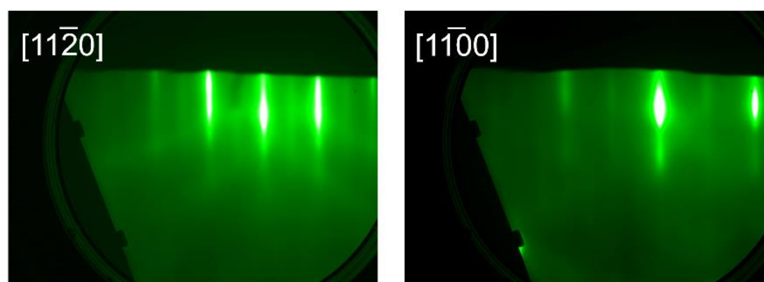

Fig. 10 — RHEED images of showing 2x2 reconstruction for MBE-grown Ga-polar GaN on MBE AlN / NbN / 4H-SiC.

Although we have thus far only demonstrated III-N polarity inversion on AlN grown on NbN, we believe it can be extended to III-N materials grown on TiN, TaN, and M_2AN materials as well though adjusting the growth conditions at the interface. Data analysis is continuing on these samples and publications are in preparation.

4. CONCLUSIONS

We have made substantial progress in the MBE growth and understanding TMN and M_2AN epitaxial films and III-N heterostructures on SiC substrates. Binary films with state-of-the-art properties were produced, and films containing Ti_2AlN were created. TaNx-based TaAlN films were also grown and their characterization is in progress. Greater understanding of the film-induced temperature rise during growth was obtained, and TiN and Si/TiN absorbing layers were created and characterized to reduce the

film-induced temperature rise and also increase thermal coupling to the substrate to enable higher-temperature film growth. Finally, a reliable technique to produce metal-polar III-N films on TMN layers by MBE was created and discussed. Understanding gained in this program has directly contributed to other research efforts, including externally funded research efforts which are on-going.

5. REFERENCES

1. https://www.mbe-komponenten.de/selection-guide/vapor-pressure.php

2. T. Joelsson *et al.*, "Single-crystal Ti_2AlN thin films," Appl. Phys. Lett. **86** 111913 (2005).

3. T. Cabioch *et al.*, "Ti_2AlN thin films synthesized by annealing of (Ti+Al)/AlN multilayers," Mat. Res. Bull. **80** 58 (2016).

4. D. S. Katzer *et al.*, "Epitaxial metallic β-Nb_2N films grown by MBE on hexagonal SiC substrates," Appl. Phys. Express **8** 085501 (2015).

5. D. S. Katzer *et al.*, "Molecular beam epitaxy of transition metal nitrides for superconducting device applications," Phys. Status. Solidi **217** 1900675 (2020).

6. C. J. K. Richardson *et al.*, "Low-loss superconducting titanium nitride grown using plasma-assisted molecular beam epitaxy," J. Appl. Phys. **127** 235302 (2020).

7. STEM imaging and analysis by Andrew C. Lang, NRL Code 6366.

8. D. S. Katzer *et al.*, "RF-plasma MBE growth of epitaxial metallic TaN_x transition metal nitride films on SiC," J. Vac. Sci. Technol. B **37** 031211 (2019).

9. A. C. Lang *et al.*, "Phase identification and ordered vacancy imaging in epitaxial metallic Ta2N thin films," ACS Appl. Mater. Interfaces, **13** 10 (2021).

10. D. S. Katzer *et al*., "Growth-induced temperature changes during transition metal nitride epitaxy on transparent SiC substrates," J. Vac. Sci. Technol. B **38** 032204 (2020).

11. M. C. Tam et al., "Temperature monitoring of narrow bandgap semiconductors," J. Vac. Sci. Technol. **B** 35 02B102-1 (2017).

12. S. R. Johnson *et al.*, "Semiconductor substrate temperature measurement by diffuse reflectance spectroscopy in molecular beam epitaxy," J. Vac. Sci. Technol. B **11** 1007 (1993).

13. W. Woltersdorff, Z. Phys. **91** 230 (1934).

14. J. F. Varner *et al.*, J. Open Res. Softw. **7** 28 (2019).

15. U. Starke *et al.*, "Morphology, bond saturation and reconstruction of hexagonal SiC surfaces," Appl. Phys. A **65** 587 (1997).

16. X. N. Xie *et al.*, "Observation of a 6x6 superstructure on 6H-SiC (0001) by reflection high energy electron diffraction," Appl. Phys. Lett. **77** 3361 (2000).

17. A. Kobayashi *et al.*, “Epitaxial junction inversion symmetry breaking AlN and centrosymmetric NbN: A polarity control of Wide-bandgap AlN,” ACS Appl. Electron. Mater. **5** 240 (2023).

18. A. Roshko *et al.*, “The role of Si in GaN/AlN/Si(111) plasma assisted molecular beam epitaxy: polarity and inversion,” Jpn. J. Appl. Phys. **58** SC1050 (2019).

19. P. Wang *et al.*, “Interfacial modulated lattice-polarity-controlled epitaxy of III-nitride heterostructures on Si(111),” ACS Appl. Mater. Interfaces **14** 15747 (2022).

20. P. Dang *et al.*, “An all-epitaxial nitride heterostructure with concurrent quantum Hall effect and superconductivity,” Sci. Adv.**7** eabf1388 (2021).